A NUMERICAL INVESTIGATION ON INGESTED WATER SEPARATION IN MODERN TURBOFAN ENGINES

V. Tasdelen, J. Hertel, R. Fiola
Rolls-Royce Deutschland Ltd. & Co. KG
Eschenweg 11
15627 Blankenfelde-Mahlow, Germany
volkan.tasdelen@rolls-royce.com

S. Staudacher
Institute of Aircraft Propulsion Systems
University of Stuttgart
Pfaffenwaldring 6
70569 Stuttgart, Germany

Abstract

Liquid water in the airflow can adversely affect the engine performance and operability. During rainy conditions, the fan module is the first component which is affected by the ingested water. The water droplets collide with the spinner as well as the fan blades and splash, spread or rebound. Due to the droplet-wall-collisions, the initial droplets breakup into smaller secondary droplets that will tend to follow the airflow. The fan rotation and droplet-wall-collisions lead to a redistribution of the amount of water in the core and in the bypass stream. In order to account for the phenomena mentioned above, a numerical approach is proposed to estimate the amount of water and its properties as it enters the core. This paper presents a two phase modelling strategy via the Lagrangian frame of reference. The flow-field solver is coupled with a droplet tracking model and breakup model. In the first step, the two phase model is introduced. In the next step, the behaviour of different droplet sizes in a generic fan geometry is examined. In addition, the effect of different water-air-ratios, initial droplet diameters and fan rotational speeds on the distribution of water between the bypass and the core has been investigated. Moreover, validation strategies are proposed and the results are compared against available experimental data from the literature.

NOMENCLATURE

Abbreviations

EASA	European Aviation Safety Agency
SWA	Separated Water Amount
T30	Compressor exit temperature
WAR	Water-Air Ratio

Indices

g	gaseous phase
l	liquid phase (droplet)
y^+	non-dimensional wall distance
y, z	coordinate

Symbols

n	droplet shape characterisation
c	velocity
c_D	drag coefficient
d_1	initial droplet diameter
d_2	droplet diameter after splashing
d_h	hydraulic droplet diameter
d_{ref}	reference droplet diameter (4096µm)
F_α	*centrifugal force*
F_D	*drag force*
g	*acceleration of gravity*
La	*Laplace number*
$\dot{m}$	*massflow*
µ	*dynamic viscosity*
Oh	*Ohnesorge number*
σ	*surface tension*
ω	*angular velocity*
Re	*Reynolds number*
ρ	*density*
S	*Splashing parameter*
We	*Weber number*

1. INTRODUCTION

Modern aero engines are expected to operate under different environmental conditions for ever increasing lengths of time while keeping safety and reliability paramount priorities. Water in the form of rain is a

perennial environmental factor. Aero engines are designed to resist water ingestion even under severe weather conditions without adversely affecting engine performance and operability. To this end, engine manufacturers are obliged to demonstrate compliance against rain before the engine goes into service [6].

The fan calculations are crucial to determine the amount of water and its properties entering in the engine core. During rainy conditions, non-uniformly distributed water droplets enter the inlet as illustrated in figure 1. Depending on the droplet diameter and its concentration, water droplets may not follow the air streamlines. The resulting slip velocity between the droplet and air leads to additional viscous drag forces. When the shear forces exceed the surface forces, the droplet will breakup into smaller droplets [17]. As proposed by Meacock [24], droplet breakup occurs already for droplet sizes up to 5µm. The rain droplets can reach a diameter of 0,5mm to 7mm. The mean diameter of rain droplets is 2,66mm [7].

The droplet breakup starts in the inlet due to the airstream acceleration and the resulting slip velocity increase. In the inlet plane, a significant amount of rain droplets impact the fan spinner and will splash, spread or rebound. Aretakis [3] has reported that approximately 20% of the initial amount of water impinges on the spinner surface. In addition, water fractions stick to the spinner surface and form a film. The water film is centrifuged towards the casing and may enter the engine core. Regarding the fan rotor, the secondary droplets derived by the spinner collisions are centrifuged toward the casing due to their small inertia [24]. Furthermore, a certain amount of the secondary droplets goes on to impact with the rotor walls, which then produces even smaller droplets. The droplet-droplet and droplet-wall collisions together with the fan rotation lead to a new distribution of the ingested water between the bypass and the core.

Computational Fluid Dynamics (CFD) tools can provide valuable support for modelling two-phase flows in turbo-machinery. However, due to the complex phenomena of two-phase flows and the interaction of the phases, the reliability of CFD results is limited. For this reason, a validation strategy has to be proposed.

2. PHENOMENA OF RAIN DROPLETS

2.1. Scoop effect

The flight condition has a significant effect on the water concentration entering the engine. During descent idle when low rotational speeds and high aircraft speeds occur, the air capture stream tube becomes smaller than the geometric inlet area. Due to the ballistic behaviour of rain droplets, the water concentration in the fan entry plane increases significantly. As a consequence, the water concentration in the inlet is higher than in the atmosphere. This phenomenon is called scoop effect [18]. The rain certification tests are made for maximum water concentrations of 20 g/m^3, which is equal to a water-air ratio of 3%. Nevertheless, the EASA proposes a water-air ratio of 4% as a maximum to compensate any flight effects [6]. The amount of water is simulated by equal sized droplets, which are ingested at the inlet entry.

2.2. Droplet Breakup

If a water droplet surrounded by air moves within a two-phase flow, droplet breakup may occur and leads to a droplet decrease. The droplet breakup process is divided into five steps (see figure 2). First, the spherical droplet shape deforms to an elliptic shape normal to the flow direction. In the next step, the elliptic shape is formed into to a bag shape due to the acting shear forces. If a critical velocity slip is reached, the bag shape will change to a hollow bag and eventually breakup into smaller secondary droplets [12]. This process is highly dependent on the aerodynamic and surface tension forces [1].

The droplet breakup is addressed by the Weber number

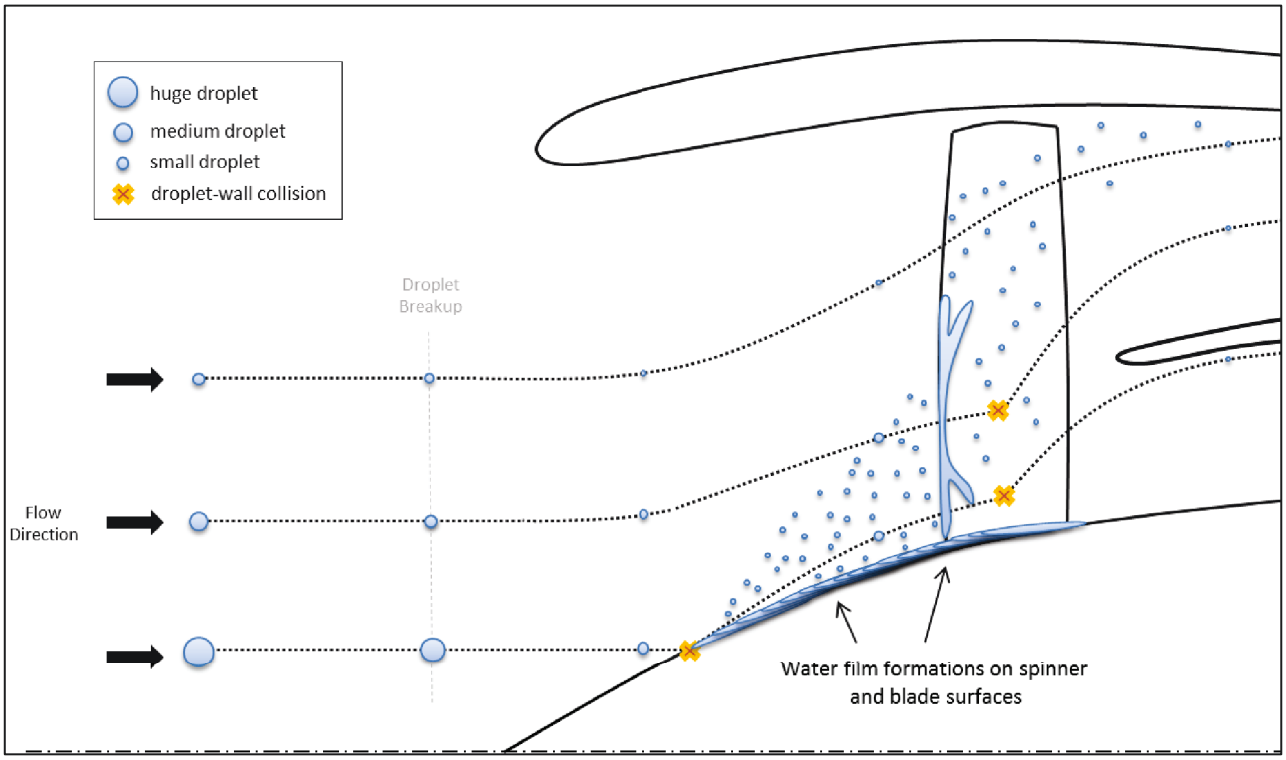

Figure 1: Schematic droplet trajectories and collisions for different droplet sizes

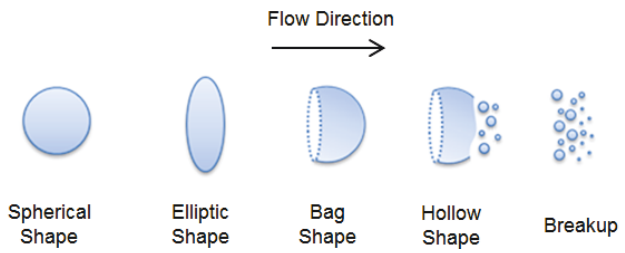

Figure 2: Droplet breakup process

and Ohnesorge number [24]. For spherical droplets, the Weber number and Ohnesorge number are defined as follows:

$$We = \frac{\rho\,(c_l - c)^2 d_1}{\sigma} \tag{2.1}$$

$$Oh = \frac{\mu_l}{\sqrt{\rho_l\, d_1 \sigma}} \tag{2.2}$$

The droplet Weber number represents the relationship between the aerodynamic force and the surface tension, whereas the Ohnesorge number considers the influence of the droplet viscosity μ_d. The surface tension is important for the droplet coherence. If the critical Weber number is exceeded, the specific breakup mechanism is assumed. Several researchers have analysed the droplet breakup mechanism for different conditions [10, 12]. In addition, Pilch and Erdman [19] have reported a droplet breakup criteria by taking into account both the Weber number and Ohnesorge number (table 1).

Breakup process	Critical Weber Nr
Bag Breakup	$12 * (1 + 1{,}077 * Oh^{1{,}4})$
Transition to multimode breakup	$20 * (1 + 1{,}20 * Oh^{1{,}6})$
Transition to shear breakup	$32 * (1 + 1{,}5 * Oh^{1{,}4})$

Table 1: Droplet breakup criteria [19]

2.3. Droplet-Droplet & Droplet-Wall Collisions

Water droplets in a water laden airflow can collide with each other and with structural parts. The droplet-droplet interaction produces smaller secondary droplets or leads to change momentum direction [2].

As shown in figure 3, the droplet-wall collisions are generally divided into three categories. The entering water droplets collide with structural parts and form a water film (Spreading), bounce and keep its initial droplet size (Rebound) or breakup into smaller droplets and re-enter the working stream (Splashing). The splashing process depends on the initial droplet size, its velocity, the fan speed and the relative position of the droplet to the fan [17].

2.4. Water Film Formations

If splashing occurs, smaller secondary droplets are produced and a liquid film on the associated wall is formed. The water film may be centrifuged towards the casing and re-enter the working stream, evaporate or move downstream into the engine core. The water film decelerates due to the drag force and surface friction. The acting centrifugal forces on the water films maintain a radial velocity and also move the water towards the casing. Das [4] has numerically investigated the water film formation on booster rotor blades. He concludes that film formations occur on the blade pressure surface for WAR up to 2%. Water film formation on blades is equivalent to a 'virtual' profile thickening and leads to a decrease in efficiency. Several authors provide correlations to estimate the water film thickness on surfaces [9, 12, 15, 20, 25]. The water film thickness could be used to address the additional profile losses.

3. TWO PHASE MODEL

There are two approaches available to model two phase flows: The Euler-Euler approach and the Euler-Lagrange approach. The schematic illustration of these two approaches is shown in figure 4. The Euler-Euler approach handles the carrying gas and the water droplets as a continuum. In this case, the two-phase flow is described by thermodynamic and fluid mechanic state variables at every time step. Due to the assumption of the fluid as a continuum, the basic equations of motion are derived in a stationary frame of reference (*Euler frame of reference*). In contrast to the Euler-Euler approach, the water droplets in the Euler-Lagrange approach are calculated in a moving frame of reference (*Lagrange frame of reference*). In this case, the water droplets and the continuous phase are in interaction, which enables the consideration of momentum and heat exchange between the two phases.

The Euler-Euler approach calculates the trajectories of each water droplet individually. This results in an increased number of equations to be solved. On the contrary, the Euler-Lagrange approach groups the water droplets to a finite number of individual droplets (parcels). Each parcel trajectory represents a number of droplets in the flow-field. The Euler-Lagrange approach is adopted in order to reduce the computing time. Besides, this model is recommended for water-air ratios less than 10% [13].

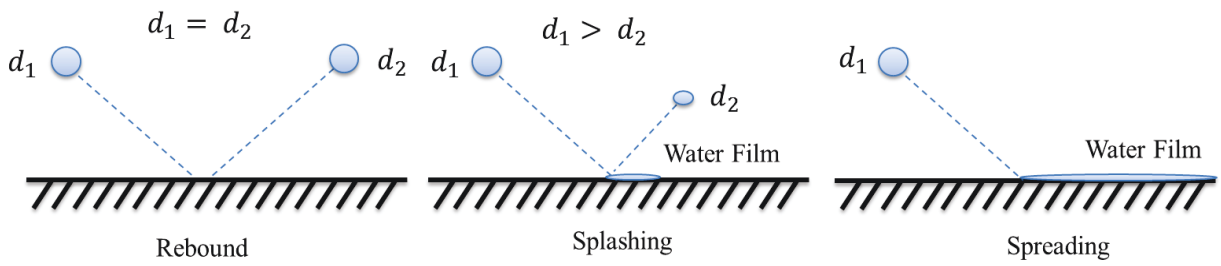

Figure 3: Mechanisms of droplet-wall collisions

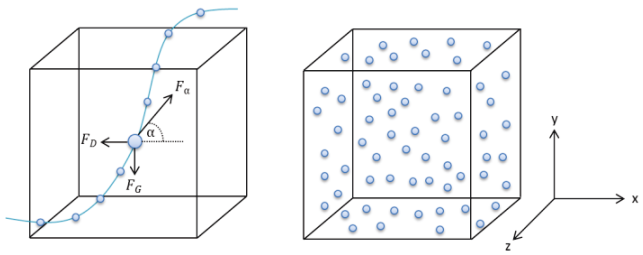

Figure 4: Euler-Lagrange Approach (left) and Euler-Euler Approach (right)

3.1. Disperse Phase Model

The two-phase flow is modelled as water droplets carried by the surrounding air. The droplet velocity along the trajectory is calculated by the temporal integration of the equilibrium of forces. The acting forces are gravitational force, drag force and centrifugal force in rotating systems:

$$\frac{dc_l}{dt} = F_D(c - c_l) + \frac{g\,(\rho - \rho_l)}{\rho_l} + F_\alpha \qquad (3.1)$$

The additional drag shear force due to the slip velocity is accounted via:

$$F_D = m\frac{d(c_l - c)}{dt} \qquad (3.2)$$

By considering the slip velocity, the total drag force can be calculated as:

$$F_D = \frac{1}{2}C_D\frac{d_1^2}{4}\rho\,(c_l - c) \qquad (3.3)$$

The Reynolds number for droplets is defined as:

$$Re = \frac{\rho\, d_h(c_l - c)}{\mu} \qquad (3.4)$$

Several authors provide correlations to estimate the drag coefficient by considering the influence of droplet deformation [14, 21, 23]. Derhoumi et al. [5] have compared the three correlations and recommends the use of Morsi and Alexander's [14] drag coefficient correlation. On the basis of experimental data, Morsi and Alexander [23] have derived the following equation:

$$C_D = \frac{24}{Re}(1 + a_1 * Re^{a_2}) + \frac{{}_3 * Re}{{}_4 + Re} \qquad (3.5)$$

The correlation in (3.5) is applicable to all particle relaxation time scales and Reynolds numbers which are considered in this study. The coefficients a_1, a_2, a_3 and a_4 are a function of the droplet shape and the Reynolds number [14].

The separation of water droplets from the two-phase flow can only occur if additional external forces act on the two phase flow. F_α describes the centrifugal force, which influences the movement of water droplets in rotational systems. The centrifugal force causes a radial velocity that moves the water droplets towards the casing. Due to the rotation around the x-axis, the centrifugal force influences the droplet trajectories in y- and z-direction respectively as follows:

$$1 - \frac{\rho}{\rho_l}\omega^2 z + 2\omega(c_{y,l} - \frac{\rho}{\rho_l}c_y) \qquad (3.6)$$

$$1 - \frac{\rho}{\rho_l}\omega^2 y + 2\omega(c_{z,l} - \frac{\rho}{\rho_l}c_z) \qquad (3.7)$$

In addition to the equations (3.1) to (3.7), Navier-Stokes equations for dry air are considered. The resulting system of equations is then numerically solved and the droplet trajectories are calculated.

3.2. Numerical Setup & Simplifications

A generic fan module of a modern turbofan engine is numerically investigated. Figure 5 illustrates the analysed fan geometry, which includes the spinner, splitter and rotor blades. The fan geometry is assumed to be rotation-symmetric. In order to reduce computing time, only a cutout of 30 degrees has been modelled.

Rain is modelled as a two-phase flow that consists of dry air and water droplets. In reality, water vapour is present as a third phase in the surrounding gas. For the present investigation, water vapour is neglected. The numerical calculations have been done for different initial droplet diameters, water-air ratios and fan speeds. It has to be noted that this investigation does not consider solid water phases (i.e. ice crystals or hail stones). The predicted droplet sizes at the splitter entry in chapter 4 are only derived by the droplet-droplet and droplet-wall collisions. Decrease of droplet size due to heat transfer between the two phases is neglected.

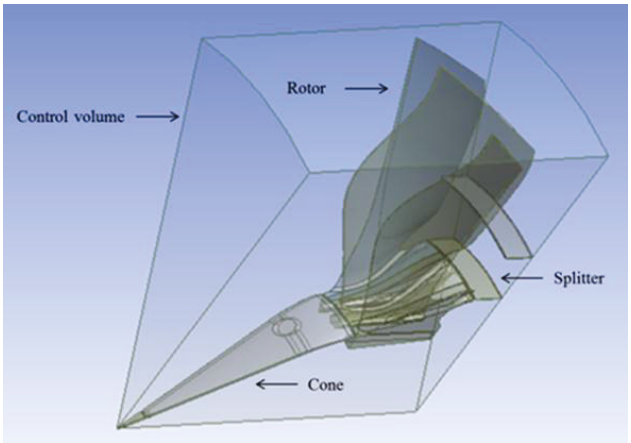

Figure 5: Cutout of a generic geometry

The fan flow-field is calculated in 3D using the k-ε turbulence model. The solver is coupled with a droplet model to estimate the droplet trajectories. Further a breakup model is used to account for water film formations as well as droplet-droplet and droplet-wall collisions and the resulting secondary droplets. The 3D calculations consider a constant droplet size until droplet breakup or droplet-wall collisions occur. The disperse phase is modelled as uniformly distributed water droplets with a temperature of 300K. The k-ε turbulence model is used with turbulence intensity values of 1 (medium intensity). Furthermore, the segregated flow model (1. Order) coupled with the Reynolds averaged Navier Stokes (RANS) equations are applied.

The splitter and the spinner are modelled as a bended surface. Due to its elementary geometry, both are meshed with hexaeder elements. Hexaeder elements require less storage capacity and converge faster than polyhedron elements. The fan rotors are more complex geometries and therefore are meshed with polyhedron elements. The total number of cell elements is 10^5.

The wall-near region is modelled with the enhanced wall treatment model to consider separation effects [11]. The non-dimensional wall distance y^+ for the wall-bounded flow is a criterion for assessing the mesh quality. If the *low-reynolds approach* is used, y^+ values less than 1 are recommended. If a *high y^+ approach* is chosen, y^+ values higher than 30 should be achieved. For the third approach, *All y^+*, values should (ideally) lie between 1 and 30 [8]. The mesh is designed to enable simulations with low and high Reynolds numbers (see table 2). For this reason, the *All y^+* approach is used. The characteristic length of the Reynolds number refers to the run length (Spinner and Splitter) and the chord length (Fan rotor blade), respectively.

Part	Re_{low}	Re_{high}
Spinner	2208	33653
Fan	1656	28236
Splitter	2489	35579

Table 2: Range of Reynolds numbers for the spinner, fan and splitter

To achieve y^+ values between 1 and 30, the mesh for the spinner, splitter and fan rotors are modified separately. The average cell size is 2mm. The boundary layer thicknesses for the three parts are listed in table 3. The mesh has a maximum skewness angle of 71,27°, a face validity of 1 and a volume change between 4,15e-004 and 1e+000. The mesh quality criteria are conformed according to the recommendations in [2].

Part	Total boundary layer thickness
Spinner	2,8 mm
Fan	2,1 mm
Splitter	3,2 mm

Table 3: Boundary Layer thickness for Re_{high}

The Lagrangian model is implemented to estimate the droplet trajectories through the flow-field. The solver does not consider individual particles. Water droplets are represented as a group of droplets which may follow the same path. For this reason, the predicted droplet trajectory is assumed as average droplet trajectory for the appropriate droplet group. In addition, the Lagrangian tracking model considers the interaction between the continuous phase and disperse phase (two-way coupling). The influence of the water droplets on the fluid-flow is accounted by the droplet source terms in the momentum equations. In addition, the Eularian Wall Film model is used to predict liquid films on the spinner surface.

4. RESULTS

The separated amount of water is calculated for several water-air ratios, fan speeds and initial droplet diameters. The value of the water-air ratio entering the core WAR_{core} is evaluated at the splitter entry plane and is averaged over the HPC area (see figure 6):

$$SWA = 1 - \frac{WAR_{core}}{WAR} \tag{4.1}$$

It has to be noted that the secondary droplet size at the splitter entry is only governed by the droplet-wall collisions and the process by which the droplet breaks up. In reality, the secondary droplet size is also changing due to heat exchange between the two phases. An additional analysis which takes into account the heat exchange between the phases was carried out to estimate the influence on the droplet size. The temperature increase of the continuous phase after the fan rotor is approximately 45K at full speed conditions and a relaxation time of $1{,}5 \cdot 10^{-3}$ seconds. Under these conditions, the droplet size decreases by less than 0,72% of its original size as a result of the heat input. Due to the minor effect of evaporation on the droplet size, heat exchange is not considered in this study.

4.1. Effect of water-air ratio

The CFD analysis is investigated for different water-air ratios between 1% and 10%. The water-air ratio is defined as follows:

$$WAR = \frac{\dot{m}_l}{\dot{m}_g} \tag{4.2}$$

The calculated separated amounts of water are reported in table 3 for water-air ratios of 1%, 5% and 10%. The results show that the separated amount of water increases slightly with higher water amounts. Change in water-air ratio from 1 to 10% results in an increase of 0,5% in the separated amount of water. Droplet-droplet collisions increase with higher water concentrations and produce smaller droplets. The droplet-droplet collisions lead to a droplet decrease from originally 1mm to 0,89mm for a water-air ratio of 1%. By increasing the water-air ratio to 10%, the averaged secondary droplet diameter decreases to 0,62mm. Smaller droplets have less inertia and lead to the higher separation rate. Due to the minor dependency between the initial amount of water and the resulting separated amount of water, the variation of water-air ratio is neglected in further calculations. All subsequent calculations are investigated with a water-air ratio of 4%.

WAR	Fan speed	d_2	**SWA**
1%	60%	0,89mm	**55.7%**
5%	60%	0,73mm	**55.9%**
10%	60%	0,62mm	**56.2%**

Table 4: Separated amount of water for water-air ratios of 1%, 5% and 10% at d_1 = 1mm

4.2. Effect of fan speed

In contrast to the water-air ratio, the fan speed has a significant effect on the separated amount of water. Figure

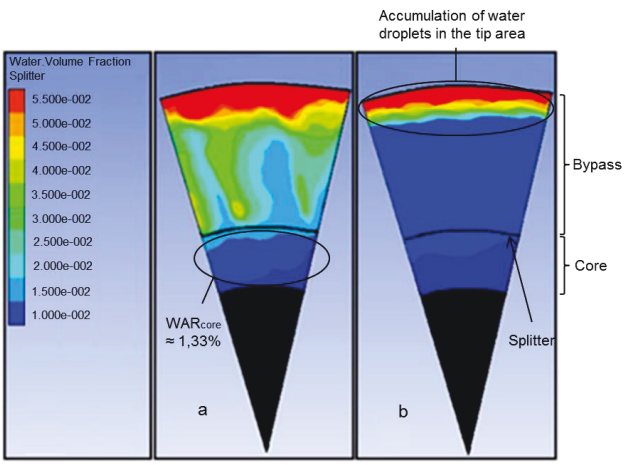

Figure 6: Radial water distribution for fan shaft speeds of 60% (a) and 100% (b), WAR = 4%, d1 = 3mm

6 illustrates the radial water distribution for a fan speed of 60% (a) and 100% (b). For a speed increase from 60% to 100%, the water-air ratio entering the core decreases from 1,33% to 1,14% with an initial droplet diameter of 3mm. The higher the fan speed, the higher the centrifugal forces, which lead to an increasing separation rate. In addition, it has been discovered that for high fan speeds the separated water is accumulated in the tip area (see figure 6b). The fan speeds are varied between 50% and 100%. An approximately linear dependency between the fan speed and the separated amount of water was observed for all initial droplet diameters as stated in figure 7.

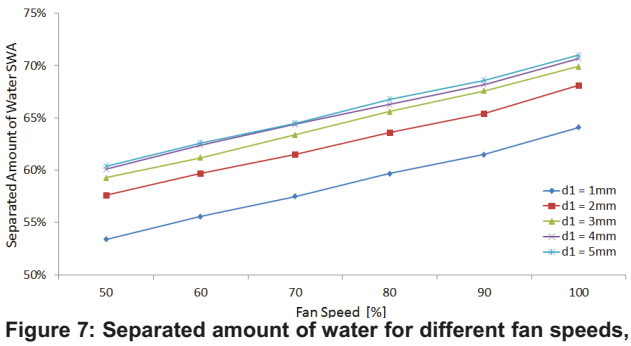

Figure 7: Separated amount of water for different fan speeds, WAR = 4%

4.3. Effect of droplet diameter

Droplet diameters are also varied to identify their effect on the separated amount of water. For this reason, the numerical investigation was performed for initial droplet diameters between 1mm and 5mm. Figure 8 shows the CFD results for droplet diameters of 1mm (a) and 3mm (b). By increasing the initial droplet diameter from 1mm to 3mm, the water-air ratio entering the core decreases by 0,64%. Figure 9 shows the predicted separated amount of water as a function of the initial droplet diameter. It has been discovered that the separated amount of water increases with higher initial droplet diameters. This trend was observed for every droplet diameter and is counter intuitive as a droplet of higher diameter would have a higher inertia and therefore require higher centrifugal forces to affect the droplet trajectories. However, this phenomenon was explained by the discovery of the droplet-wall collisions producing smaller secondary droplet sizes. It is observed that the higher the initial droplet

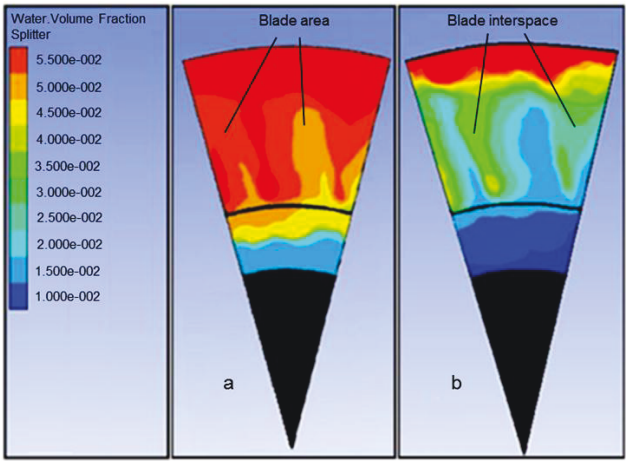

Figure 8: Radial water distribution for an initial droplet diamater of 1mm (a) and 3mm (b), WAR = 4%, 60% fan speed

diameter, the smaller the secondary droplet size at the splitter entry plane. Smaller droplets have a smaller inertia and lead to the increase in the water entering the bypass. The droplet size after splashing is discussed in section 5.1.

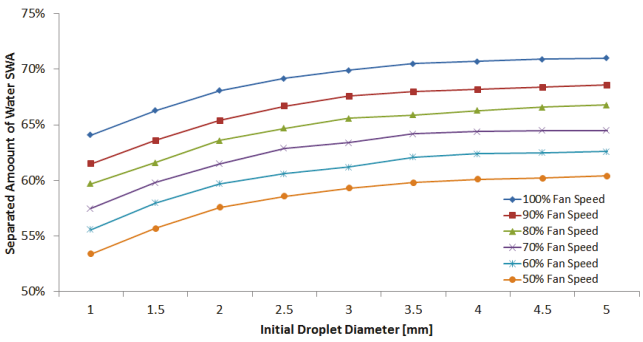

Figure 9: Separated amount of water for different initial droplet sizes, WAR = 4%

4.4. Film Formation on the spinner surface

Droplets that impinge on structural parts form a liquid film. The liquid film is decelerated due to the drag force and surface friction. As a result, some fractions of the water re-enters into the working stream in the form of large droplets.

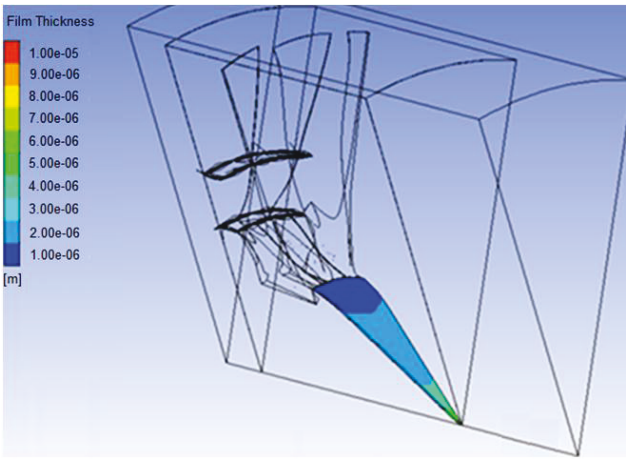

Figure 10: Water film thickness on fan spinner, WAR = 4%, d_1 = 3mm initial droplet diameter, 60% fan speed

It has been discovered that significant film impingements only occur on the spinner surface. The resulting water film thickness depends on the ingested water amount, the fan speed and the spinner geometry. Figure 10 shows the water film thickness on the spinner surface for a fan speed of 60% and a water-air ratio of 4%. On the spinner front, a film thickness of 10µm is estimated. The water film thickness decreases with increasing axial direction and is approximately 1,1µm in the spinner-blade intersection. The higher the radius, the higher the local circumferential force and the lower the resulting film thickness.

5. VALIDATION STRATEGY

5.1. Secondary droplet size

The predicted secondary droplet size is compared to data available from literature. Schmehl [22] has investigated the splashing process of water droplets in industrial gas turbines. He has developed a correlation based on empirical data to assess the resulting droplet diameter after droplet-wall collisions and is valid for a wide range of Laplace numbers ($0 \leq La \leq 10^5$):

$$\frac{d_1}{d_2} = exp(-2 - \frac{d_1}{d_{ref}} - 0{,}05 \cdot S) \qquad (5.1)$$

S is the *Splashing* parameter, which is a modification of the Weber number. The *Splashing* parameter *S* is used to identify the outcome of the droplet-wall collision (table 4). *Splashing* occurs, if *S* > 1:

$$S = \frac{Re}{24 \cdot La^{0,419}} \qquad (5.2)$$

$$La = \frac{\rho_l \, d_1 \, \sigma}{\mu_l^2} \qquad (5.3)$$

Regime	Weber Number	Splashing Parameter
Rebound	5 < We < 10	S < 1
Spreading	We > 10	S < 1
Splashing	-	S > 1

Table 5: Splashing criterion according to Schmehl [22]

The predicted result for the secondary droplet size is compared with the correlation from Schmehl (see figure 11). Both the simulation results and Schmehl's correlation show the same trend. The higher the initial droplet diameter, the smaller the secondary droplet size after splashing. It has been found that after splashing the original droplet size decreases by a factor of 50-100. It has to be noted that the produced secondary droplet size is highly dependent on the initial droplet velocity. The presented investigation was performed for an initial droplet velocity of 250 knots at the inlet entry which is also assumed for the engine certification tests with water ingestion.

Figure 12 illustrates the deviation between the predicted secondary droplet size and the correlation of Schmehl:

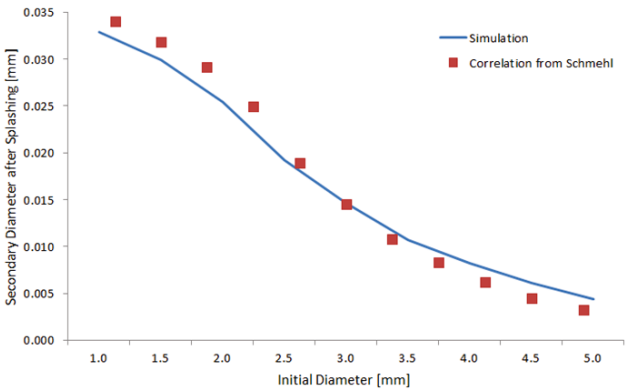

Figure 11: Comparison of d2 in denpendence on d1 with the correlation of Schmehl

$$Deviation = \frac{d_{Simulation} - d_{Schmehl}}{d_{Simulation}} * 100\% \qquad (5.4)$$

The deviation is at a maximum of 3,3% for an initial droplet diameter of 1mm. The difference gradually diminishes and at 3,3mm, the difference becomes negative. It has been observed that this trend continues and reaches a maximum deviation of -2,4% at an initial diameter of 5mm.

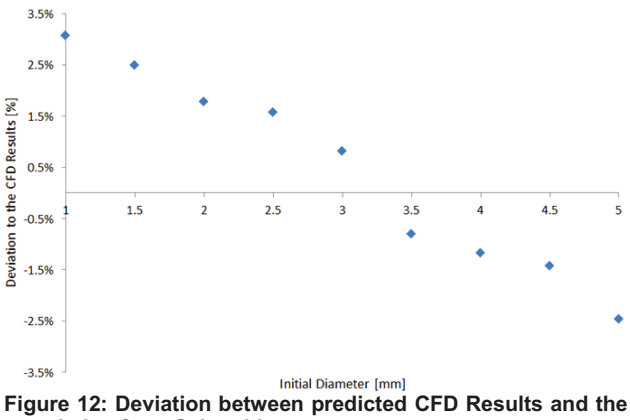

Figure 12: Deviation between predicted CFD Results and the correlation from Schmehl

The observed deviation in figure 12 is explained by the validity interval of Schmehl's correlation. Figure 13 shows that the predicted Laplace numbers for droplets greater than 3,3mm surpasses the limit of $La_{max} = 10^5$.

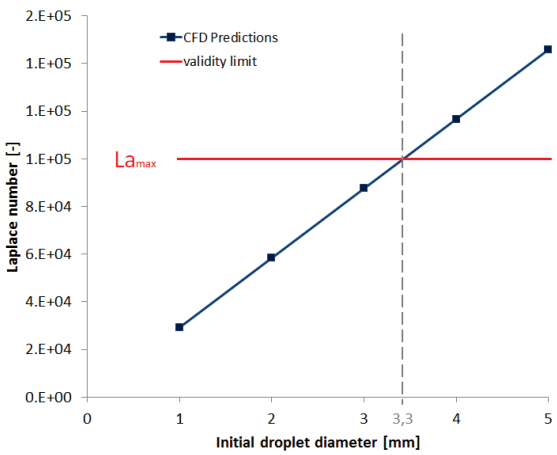

Figure 13: Predicted Laplace numbers compared to the validity limit of Schmehl

5.2. Separated amount of water

The validation strategy for the separated amount of water is illustrated in figure 14 and requires test data from a water ingestion test as well as a wet compression model. The wet compression model enables the prediction of stage characteristics with water injection for a multistage compressor and could be similar to [3] or [24]. The first step is to ensure that the test data is obtained from a water ingestion test carried out on an appropriate engine. For the water ingestion tests, the water is ingested in front of the fan module.

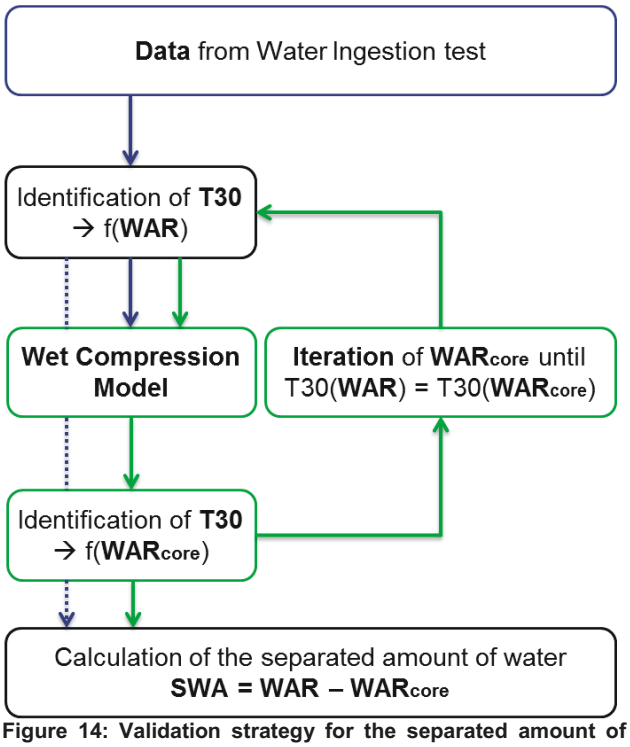

Figure 14: Validation strategy for the separated amount of water

Based on the ingested water quantity, the compressor outlet temperature (T30) is measured. In the next step, the wet compression model is used to predict the resulting compressor outlet temperature at the same ingested water quantity. In contrast to the water ingestion test, the wet compression model is able to ingest the water after the fan into the engine core. The ingested water-air ratio in the wet compression model is iterated until the same compressor outlet temperature is achieved as in the water ingestion test. In the last step, both water-air ratios are compared and the separated water amount is calculated by the difference of both water-air ratios. The resulting water-air ratios can then be compared with the CFD results and the deviation determined. This methodology can only be used if droplet evaporation is neglected and the Handling Bleed Valves are closed during the engine test.

6. CONCLUDING REMARKS

The mathematical modelling and analysis of rain water ingestion and its effects on a modern fan module was undertaken with the primary aim of identifying the parameters that control the segregation of water between the core and the bypass duct. In the past, the ratio of water entering the core and bypass were assumed as being equal to the bypass ratio. It has been discovered that this assumption does not apply for the higher end of the engine operating range. It has been shown that the core to bypass water split is dependent on the initial droplet diameter and the fan speed. Furthermore, the core to bypass water split has a weak dependency on the water-air ratio which has been neglected at this stage.

In general, secondary droplet sizes are not measured on water ingestion tests. Due to the lack of test data, the secondary droplet size has been compared to available correlations from literature. It has been shown that the predicted sizes of secondary droplets conform to the correlation of Schmehl. The use of Schmehl's correlation is limited, because variable geometries are not considered in his investigation. Further, the correlation is not valid for the entire operating range. For an in-depth validation, it is proposed to use a laser measurement method for estimating the secondary droplet size after the collisions. This approach would provide more reliable results.

ACKNOWLEDGEMENTS

The author thanks Prof. S. Staudacher, Prof. R. Fiola and Dr. J. Hertel for their support and their comments on this paper. I also want to thank Rolls-Royce Deutschland for providing the opportunity to perform this research work.

REFERENCES

[1] W.H. Anderson and H.E. Wolfe: *Aerodynamic Breakup of Liquid Drops*. In: Proceedings of 5th International Shock Tube Symposium. Ohio, 1965

[2] *Ansys Fluent Theory Guide*

[3] H. Aretakis and K. Mathioudakis: *Development and Integration of Rain Ingestion Effects in Engine Performance Simulations*. In: Proceedings of ASME Turbo Expo, ASME Turbo Expo 2014, GT2014-26556. Düsseldorf, 2014

[4] K. Das; A. Hamed and D. Basu: *Droplet trajectories and collection on fan rotor at off-design conditions*. In: Proceedings of ASME Turbo Expo, ASME Turbo Expo 2006, GT-2006-91214. Barcelona, 2006

[5] Z. Derhoumi; P. Mandin, R. Wuthrich and H. Roustan: *Experimental and Numerical Investigations of Two-Phase Electrolysis Processes - Electrical Energy Conversion in Hydrogen Production*. In: Journal of Applied Fluid Mechanics, Vol. 4, 2011

[6] European Aviation Safety Agency: *Certification Specifications for Engines CS-E*. Amendment 3. 2010

[7] European Aviation Safety Agency: *Certification Standard Atmospheric Concentrations of Rain and Hail*. Appendix A. 2013

[8] J.H. Ferzinger and M. Peric: *Numerische Strömungsmechanik*. In: Springer Verlag. Berlin, 2002

[9] G. Gyarmathy: *Theory for wet steam turbines*. In: Institute for thermal turbomachines, Federal Technical University. Zürich, 1962

[10] J.B. Kennedy and J. Roberts: *Rain Ingestion in a Gas Turbine Engine*. In: 4th Annual Conference ILASS-AMERICAS Institute of Liquid Atomization and Spray Systems. Hartford, 1990

[11] M. Kriegel: *Experimentelle Untersuchung und numerische Simulation eines Quellluftsystems*. Technische Universität Berlin, PhD Thesis. Berlin, 2005

[12] H. Liu: *Science and Engineering of Droplets*. In: 1st edition of Noyes Publications. New York, 2000.

[13] A. Matysiak: *Euler-Lagrange Verfahren zur Simulationtropfenbeladener Strömung in einem Verdichtergitter.* Universität der Bundeswehr Hamburg, PhD Thesis. Hamburg, 2007

[14] S.A. Morsi and A. J. Alexander: *An Investigation of Particle Trajectories in Two-Phase Flow Systems*, Journal of Fluid Mechanics, 1972

[15] C. Mundo; M. Sommerfeld and C. Tropea: *Droplet-Wall Collisions: Experimental Studies of the Deformation and Break Up Process.* In: International Journal of Multiphase Flow,1995

[16] T. Nikolaidis: *Water Ingestion Effects on Gas Turbine Engine Performance.* Cranfield University, PhD Thesis, Cranfield, 2008

[17] M. Obermüller; K.J. Schmidt and D. Peitsch: *Some Aspects on Wet Compression - Physical Effects and Modeling Strategies used in Engine Performance Tools.* In: Deutscher Luft- und Raumfahrtkongress, DLRK-2012-281210. Berlin, 2012.

[18] Propulsion and Energetics Panel Working Group 24: *Recommended Practices for the Assessment of the Effects of Atmospheric Water Ingestion in the Performance and Operability of Gas Turbine Engines / AGARD*. In: Canada Communication Group, AGARD-AR-332. Québec, 1995

[19] M. Pilch and C.A. Erdman: *Use of Breakup Time Data and Velocity History Data to Predict the Maximum Size of Stable Fragments for Acceleration-Induced Breakup of a Liquid Drop*. In: International Journal of Multiphase Flow, 1987

[20] W. Samenfink; A. Elsaber; K. Dullenkopf and S. Wittig: *Droplet interaction with shear-driven liquid films: analysis of deposition and secondary droplet characteristics*. In: International Journal of Heat and Fluid Flow, 1999

[21] L. Schiller und Z. Naumann: *A Drag Coefficient Correlation*. Zeitschrift des Vereines Deutscher Ingenieure, Vol. 77, 1933

[22] R. Schmehl; H. Rosskamp; M. Willmann and S. Wittig: *CFD analysis of spray propagation and evaporation including wall film formation and spray film interactions*. In: International Journal of Heat and Fluid Flow, 1999.

[23] M.J. Schuh; C.A. Schuler and J.A.C. Humphrey: *Numerical calculation of particle-laden gas flows past tubes*, AIChE Journal, Volume 35, 1989

[24] A. White and A.J. Meacock: *An Evaluation of the Effects of Water Injection on Compressor Performance*. In: Proceedings of GT2010, ASME Turbo Expo 2010, GT2010-23793. Glasgow, 2013

[25] J. Williams and J.B. Young: *Movement of deposited water on turbomachinery rotor blade surfaces*. In: Proceedings of ASME Turbo Expo, ASME Turbo Expo 2006, GT2006-90792. Barcelona, 2006

[26] J. Williams: *Water ingestion in jet engines*. University of Cambridge, PhD Thesis. Cambridge, 2003